Published in final edited form as:
Sci Transl Med. 2011 July 13; 3(91): 91ra63. doi:10.1126/scitranslmed.3002304.

A Critical Subset Model Provides a Conceptual Basis for the High Antiviral Activity of Major HIV Drugs**

Lin Shen[1,2], **S. Alireza Rabi**[1], **Ahmad R. Sedaghat**[1,*], **Liang Shan**[1,2], **Jun Lai**[1], **Sifei Xing**[1,2], and **Robert F. Siliciano**[1,3,†]

[1]Department of Medicine, Johns Hopkins University School of Medicine, Baltimore, MD 21205, USA

[2]Department of Pharmacology and Molecular Sciences, Johns Hopkins University School of Medicine, Baltimore, MD 21205, USA

[3]Howard Hughes Medical Institute, Baltimore, MD 21205, USA

Abstract

Control of HIV-1 replication was first achieved with regimens that included a nonnucleoside reverse transcriptase inhibitor (NNRTI) or a protease inhibitor (PI); however, an explanation for the high antiviral activity of these drugs has been lacking. Indeed, conventional pharmacodynamic measures like IC_{50} (drug concentration causing 50% inhibition) do not differentiate NNRTIs and PIs from less active nucleoside reverse transcriptase inhibitors (NRTIs). Drug inhibitory potential depends on the slope of the dose-response curve (m), which represents how inhibition increases as a function of increasing drug concentration and is related to the Hill coefficient, a measure of intramolecular cooperativity in ligand binding to a multivalent receptor. Although NNRTIs and PIs bind univalent targets, they unexpectedly exhibit cooperative dose-response curves ($m > 1$). We show that this cooperative inhibition can be explained by a model in which infectivity requires participation of multiple copies of a drug target in an individual life cycle stage. A critical subset of these target molecules must be in the unbound state. Consistent with experimental observations, this model predicts $m > 1$ for NNRTIs and PIs and $m = 1$ in situations where a single drug target/virus mediates a step in the life cycle, as is the case with NRTIs and integrase strand transfer inhibitors. This model was tested experimentally by modulating the number of functional drug targets per virus, and dose-response curves for modulated virus populations fit model predictions. This model explains the high antiviral activity of two drug classes important for successful HIV-1 treatment and defines a characteristic of good targets for antiviral drugs in general, namely, intermolecular cooperativity.

†To whom correspondence should be addressed. rsiliciano@jhmi.edu.
*Current affiliation: Department of Otolaryngology Massachusetts Eye and Ear Infirmary Harvard Medical School Boston, MA02114, USA.

Author contributions: L.Shen and R.F.S. designed the experiments. L.Shen, J.L., and S.X. performed the experiments. L.Shen, S.A.R., A.R.S., L.Shan, and R.F.S. analyzed data. All of the authors contributed to the manuscript preparation.

Competing interests: The authors declare that they have no competing interests.

Introduction

In 1997, regimens were developed that suppressed HIV-1 viremia to below the detection limit in most treated patients. These regimens combined two nucleoside analogue reverse transcriptase inhibitors (NRTIs) with an HIV-1 protease inhibitor (PI) (1–3). Combinations of two NRTIs and a non-nucleoside reverse transcriptase inhibitor (NNRTI) also proved effective (4,5). Collectively, these regimens, known as highly active antiretroviral therapy (HAART), transformed a previously fatal disease into a chronic condition that is well controlled in adherent patients. Despite HAART's success, a fundamental theory explaining its effectiveness is lacking.

Drug resistance, which results both from the high error rate of reverse transcriptase and the dynamic nature of HIV-1 infection, is a major cause of treatment failure (6–10). The low probability of multiple simultaneous resistance mutations on the same genome clearly contributes to the success of triple combination therapy (11). However, suppression of HIV-1 replication is not simply the result of using three drugs; some triple NRTI combinations had suboptimal responses (5). Thus, in early treatment efforts, inclusion of a PI or NNRTI appeared essential for control of viral replication. Although the use of drugs acting through different mechanisms also contributes to the effectiveness of combination therapy, PIs and NNRTIs appeared to have greater antiviral activity than most NRTIs. Therefore, treatment guidelines recommend inclusion of a PI or NNRTI in most initial HAART regimens (5). Standard pharmacologic measures such as IC_{50} and inhibitory quotient do not distinguish PIs and NNRTIs from less active NRTIs (12). Thus, the fundamental pharmacodynamic principles underlying this successful treatment remain unclear. Instead, progress has depended on comparative clinical trials, which have recently established a role for newer drugs as well, such as integrase strand transfer inhibitors (InSTIs) and CCR5 antagonists (5).

We recently showed that the superior antiviral activity of PIs and NNRTIs relative to most NRTIs can be partially explained by the dose-response curve slope (m) (12). This parameter is included in all fundamental pharmacodynamic equations including the Hill equation (13), the sigmoidal E_{max} model (14), and the Chou-Talalay median effect equation (15). The slope parameter is related to the Hill coefficient describing intramolecular cooperativity in the binding of ligands to a multivalent receptor (13, 16). Positive cooperativity ($m>1$) reflects enhanced binding of additional ligands to a receptor after the first ligand binds. Interestingly, the enzymes targeted by NNRTIs and PIs are univalent with respect to these inhibitors. NNRTIs bind to a single pocket adjacent to the dNTP binding site (17), and HIV-1 protease is a homodimer with a single active site targeted by PIs, which are peptidomimetic substrate or transition state analogs (18, 19). Therefore, non-cooperative dose-response curves ($m=1$) were expected. However, in single round infectivity assays, dose-response curves for NNRTIs and PIs have unexpectedly steep slopes (~1.7 and ranging from 1.8 to 4.5, respectively), allowing these drugs to achieve extraordinarily high antiviral activity (12).

Since $m>1$ for NNRTIs and PIs cannot be explained by intramolecular cooperativity, a mechanistic explanation requires reconsidering the concept of cooperativity in drug action. Here we describe a critical subset model that explains steep slopes for these drugs in terms of intermolecular cooperativity, and we provide experimental validation for this model.

Results

The critical subset model

The simplest model describing dose-response relationships is the median effect equation (15). It is derived from the law of mass action, which governs dynamic equilibria in chemical reactions. The median effect equation can be written as:

$$\log(f_a/f_u)=m\log([D]/IC_{50}) \quad (1)$$

$$\text{or,} \quad f_a=\frac{1}{1+\left(\frac{IC_{50}}{[D]}\right)^m} \quad (2)$$

In the context of HIV-1 infection, f_a and f_u are the fractions of viruses affected and unaffected by drug, $[D]$ is drug concentration, IC_{50} is the drug concentration causing 50% inhibition, and m is the slope parameter describing the steepness of the dose-response curve.

Some anti-HIV drugs have $m>1$ even though their target enzymes are univalent. To explain this observation, we developed a critical subset model based on mass action. The model envisions independent binding of multiple drug molecules to a set of identical targets, viral proteins, within each virus or virus-infected cell. Within a given virion or infected cell, the targeted proteins behave as a set of linked receptor sites that can be occupied to variable extents (Fig. 1A), depending on $[D]$ and the affinity of individual drug-target interactions (K_d). Drug binding involves a series of equilibrium reactions mediating conversions between all possible partially occupied states (16). Assuming that replication requires some critical threshold number (c) of functional (unbound) enzyme molecules to complete the relevant reaction before irreversible decay processes intervene (Fig. 1B), the following expression describes f_a as a function of $[D]$, K_d, the unbound virus concentration $[V]$, and the total number of enzyme molecules per virus n_T (Equation 3, Table 1):

$$f_a(n_T)=\frac{\sum_{i=n_T-c+1}^{n_T}\binom{n_T}{i}[V]\left(\frac{[D]}{K_d}\right)^i}{\sum_{i=0}^{n_T}\binom{n_T}{i}[V]\left(\frac{[D]}{K_d}\right)^i}=\frac{\sum_{i=n_T-c+1}^{n_T}\binom{n_T}{i}\left(\frac{[D]}{K_d}\right)^i}{\sum_{i=0}^{n_T}\binom{n_T}{i}\left(\frac{[D]}{K_d}\right)^i} \quad (3)$$

Consider for example HIV-1 protease. Multiple copies of protease participate in the maturation of each virion. Although not physically linked, they are constrained spatially within the virion. Thus, the virion can be considered a multivalent receptor with n_T binding sites, where n_T is the total number of protease molecules per virus (Fig. 1A). Since simultaneous binding is unlikely, we have modeled drug binding as a series of equilibrium reactions (Fig. 1B). The derivation of Equation 3 follows from a consideration of the concentration of each possible state along the path to saturation (16). Viruses with a critical subset of c or more unbound enzymes are infectious. To render a virus noninfectious, at least n_T-c+1 enzyme molecules must be occupied (Fig. 1B). Thus in Equation 3, the numerator is the sum of the concentrations of all viruses having $\geq n_T-c+1$ enzyme molecules bound by drug, and the denominator is the total virus concentration.

This model predicts the shapes of dose-response curves. To illustrate these predictions, we plotted hypothetical dose-response curves using median effect plots based on Equation 1 (Fig. 2). The median effect plot linearizes the dose-response curve for most drugs, with the

slope of the resulting line equal to the Hill coefficient (Fig. 2A–B). We obtained complex dose-response curves with various m depending on n_T and c (Fig. 2C–D). Importantly, when n_T=c=1, Equation 3 simplifies to the median effect equation (Equation 2) and predicts m=1. However, for all cases with $1<c<n_T$, the model predicts steeper dose-response curves with $m \geq 1.5$ at all drug concentrations.

Interestingly, the model predicts complex dose-response curves with non-linear median effect plots. In other words, m is different for different segments of the curve. As shown below, the dose-response curves of some antiretroviral drugs are similarly complex. According to the model, slope values are determined by n_T and c. As [D] increases above IC_{50}, m approaches c. As [D] decreases below IC_{50}, m approaches $n_T - c+1$ (Supplementary Note 1). Within the range of log (f_a/f_u)= −2 to 4 (1–99.99% inhibition), the curves inflect upward when c is close to n_T and downward when c is small relative to n_T (Fig. 2C–D). For example, when n_T=5, the model predicts a family of curves with slopes ranging from 1.30 to 1.88 at the IC_{50} (Fig. 2C). Slope at the IC_{50} is highest when c=3, and lowest when c=1 or 5. However, the slope at high [D] approaches c, and thus the maximum slope is 5. The same pattern with steeper slopes is observed for n_T=30 (Fig. 2D). Whenever simultaneous inhibition of multiple copies of a target molecule within a virion or infected cell is required to block replication, dose-response curves with m>1 are predicted by this model. This unique form of intermolecular cooperativity does not depend on changes in the binding properties (K_d) of individual target sites.

The model also predicts the relationship between IC_{50} and K_d. When n_T is odd and c=(n_T+1)/2, IC_{50}=K_d. When c>(n_T+1)/2, IC_{50} < K_d and vice versa (Fig. 2C–D). Similarly, for a series of curves with constant c, IC_{50} decreases as n_T decreases (Fig. 2E–F). This is expected because a lower IC_{50} is achieved with the same K_d when the fractional occupancy of target enzymes required for inhibition is low.

Effect of heterogeneity on dose-response curves

A second factor affecting slope is heterogeneity in n_T. In other biological systems with all-or-none outcomes, heterogeneity in the number of drug targets flattens dose-response curves (20). For individual virions, infection is all-or-none, and thus heterogeneity arguments apply. When heterogeneity is limited, dose-response curves are steeper. Intuitively, this may be understood by considering that a homogeneous virus population will be inhibited over a narrow range of drug concentrations, whereas a more heterogeneous population will contain viruses that are easier or harder to inhibit, and therefore inhibition will be observed over a wider concentration range.

If n_T follows an integer-valued normal distribution with a standard deviation σ, then dose-response curves follow Equation 4, which gives f_a for a population of viruses with variability in n_T.

$$f_a(n_T,\sigma)=\frac{\sum_{n_i=c}^{n_{\max}}[f_a(n_i)P(n_i|n_T,\sigma)]}{\sum_{n_i=c}^{n_{\max}}P(n_i|n_T,\sigma)} \quad (4)$$

where

$$P(n_i|n_T,\sigma)=\frac{1}{\sigma\sqrt{2\pi}}e^{\frac{-(n_i-n_T)^2}{2\sigma^2}} \quad (5)$$

and $f_a(n_i)$ is calculated using Equation 3. The derivation of Equation 4 follows from a consideration of f_a for viruses with a given total number of enzyme molecules per virus (n_i) and the probability of finding viruses with n_i enzyme molecules within a population of viruses with $n_T \pm \sigma$ total enzyme molecules per virus (Fig. S1A). Since viruses with $n_i < c$ are noninfectious, the numerator must be divided by the probability of infectious virus for a given n_T, σ, and c (Fig. S1A). n_{max} is the maximum total number of enzyme molecules per virus, which is set at $> n_T + 3\sigma$. Equation 4 predicts a decrease in m with increasing σ at drug concentrations below the IC_{50} (Fig. S1B), since heterogeneity leads to a subpopulation of viruses with low n_T that are inhibited more easily at low [D].

Testing the critical subset model with phenotypic mixing experiments – theoretical considerations

The critical subset model makes testable predictions about how variation in n_T and c affect dose-response curves. For example, the model predicts that at constant c, IC_{50} decreases as n_T decreases (Fig. 2E–F). To test this model, we used a phenotypic mixing strategy (21,22) to reduce the total number of functional target molecules per virion (n_F) (Fig. 3A). To reduce n_F, defined fractions (f_m) of mutant proviral constructs containing inactivating point mutations in the target enzymes were mixed with wild type constructs and transfected into HEK293T cells to generate virions with reduced n_F. Note that $n_F = n_T$ when no mutant enzyme is present. We then examined the relative infectivity (RI) of these virus populations compared to wild-type virus and obtained estimates of n_T and c (Fig. 3B–C). Finally, we determined whether the dose-response curves for virus populations with lower n_F behaved as predicted by the model (Fig. 3D–E). Note that larger decreases in IC_{50} are predicted when c is small relative to n_T.

The introduction of mutant enzyme subunits reduces infectivity, as some viruses will no longer contain a critical number of functional enzymes (Fig. 3A). The enzyme molecules targeted by RT and protease inhibitors are heterodimers and homodimers, respectively. If formation of mixed dimers from wild-type and mutant monomers follows random mixing, then the virions produced should contain reduced n_F following a binomial distribution. The RI of mixed virions compared to wild-type virions is a function of n_T, c, and P_f, where P_f is the probability of obtaining a functional enzyme multimer for a given f_m (Equation 6).

$$RI(n_T)=\sum_{n_F=c}^{n_T}P(n_F)=\sum_{n_F=c}^{n_T}\binom{n_T}{n_F}P_f{}^{n_F}(1-P_f)^{n_T-n_F} \quad (6)$$

$P(n_F)$ is the probability of getting n_F copies of functional enzyme molecules with a given n_T, c, and P_f. The calculation of P_f from f_m is based on the subunit stoichiometry of the target enzyme and is different for RT and protease, as described in Methods. Based on Equation 6, the RI of phenotypically-mixed virions is the sum of the probabilities of obtaining viruses with $n_F \geq c$. Plotting RI as a function of f_m, we obtain RI curves with various patterns depending on n_T and c (Fig. 3B–C). When most copies of the enzyme are required to complete the relevant step in the life cycle, decreases in n_F have a major effect – a small increase in f_m results in loss of infectivity. In contrast, when c is small relative to n_T and thus available enzyme exceeds that which is necessary, infectivity is not affected until f_m is large (Fig. 3B–C). As demonstrated below, the former situation applies to RT whereas the latter applies to protease. Note that the analysis of RI is based on the same assumptions that

underlie the critical subset model, namely that a critical threshold number (c) of functional copies of a viral enzyme out of n_T copies are required for infectivity (Fig. 1B, 3A).

To test the critical subset model, phenotypically-mixed viruses can be assayed for susceptibility to drug inhibition. Dose-response curves for inhibition of viruses with various f_m can be predicted by Equation 4, where the calculation of $f_a(n_i)$ follows Equation 7 (Fig. 3D–E). The derivation of Equation 7 follows from a consideration of f_a for each n_F (Equation 3) and the probability of viruses with n_F functional enzyme molecules within a population of viruses with n_i total enzyme molecules and an average probability P_f of functional ones (Equation 6, Fig. 3A).

$$f_a(n_i)=\frac{\sum_{n_F=c}^{n_i}[f_a(n_F)P(n_F)]}{RI(n_i)} \quad (7)$$

According to this model, the change in IC_{50} depends on the fractional occupancy of enzyme molecules required for inhibiting replication. Two contrasting situations with the same value of c but different values of n_T are illustrated in Figures 3D and 3E. When c is close to n_T (Fig. 3D, $n_T = 5$), the fractional occupancy required for inhibition is low, and the model predicts that IC_{50} should only decrease slightly with increasing f_m. This is because the number of enzyme molecules is already close to the limiting value of $n_T = c$. However, when c is small relative to n_T (Fig. 3E, $n_T = 30$), the fractional occupancy required for inhibition is high, and the model predicts that IC_{50} can decrease over a wider range with increasing f_m until the limiting condition is reached.

Experimental validation of the critical subset model – generation of phenotypically mixed virions

Before testing the critical subset model, we validated several assumptions. One is that wild-type and mutant enzymes can be expressed in cells and incorporated into virions with similar efficiency. We chose well-characterized point mutations in the active sites of RT (D185N), protease (D25N), and integrase (D64E) that abolish enzyme activity without effects on multimer formation or virus assembly (18, 23, 24). Transfection efficiency was similar for the wild-type plasmid and mutant plasmids by flow cytometry (Fig. S2A). Wild-type and mutant RT and integrase were incorporated into the virions with similar efficiency (Fig. S2B–C). We also tested whether formation of mixed dimers from wild-type and mutant monomers follows random mixing and hence the binomial distribution. To obtain direct biochemical evidence for mixed dimer formation in cotransfected cells, we performed co-immunoprecipitations (Fig. S3). We introduced either an HA or a Flag tag into the N terminus of the wild-type and mutant enzymes. Viral proteins immunoprecipitated by either anti-HA or anti-Flag antibodies from cell lysates were immunoblotted with anti-Flag or anti-HA antibodies, respectively. Our results suggest that for both RT and protease, dimers with all of the four possible combinations – wild-type-wild-type, wild-type-mutant, mutant-wild-type, mutant-mutant – can be formed with approximately equal probability (Fig. S3A–B).

Analysis of dose-response curves for NNRTIs and PIs against phenotypically-mixed viruses

According to the model, drugs targeting steps involving multiple copies of the drug target should show steeper dose-response curves and dramatically better inhibition at drug concentrations above the IC_{50}. NNRTIs can interact with all RT molecules in the preintegration complex, and PIs can interact with all protease molecules in the maturing virion. These drug classes exhibit slopes >1.7 and high inhibitory potential (12). For

NNRTIs and PIs, the model predicts that IC_{50} should decrease as n_F is reduced and that the higher the fractional occupancy required for inhibiting replication, the greater the change in IC_{50} (Fig. 3D–E).

We tested these predictions using the algorithm shown in Figure 4A. We first determined the apparent n_T and c by measuring in the absence of drug the RI of virions with mixtures of catalytically active and inactive enzymes. The RI of phenotypically-mixed virions can be calculated with Equation 6 for any given n_T and c (Fig. 3A). We fitted experimental RI data to theoretical RI curves for RT and protease and calculated r^2 values for all combinations of n_T between 1 and 100 and c between 1 and n_T (Fig. 4B–C). The r^2 values shown in Figure 4B and 4C indicate poor fitting for n_T>50. The experimental RI curves fit the theoretical curves best with either n_T=2, c=2 or n_T=4, and c=3 for RT (Fig. 4B, D), and n_T=9–15 and c=2, for protease (Fig. 4C, E). Importantly, with these n_T and c values, the model predicts m=1.4–2.0 for NNRTIs and m>1.8 for PIs, consistent with experimental observations.

To refine values for n_T and c and find the approximate K_d, we used estimates from RI curves as a starting point to find σ and K_d values that allowed optimal fitting of dose-response curves for NNRTIs and PIs against wild-type viruses (Fig. 4A, Equations 4–7, Supplementary Note 2). For NNRTIs, n_T=4, σ=1, c=3 gave the best average fit (Fig. 5A), with K_d=0.018 μM, 0.33 μM, and 0.018 μM for efavirenz (EFV), nevirapine (NVP), and etravirine (ETR), respectively. The inclusion of σ for RT improved the fitting of the RI curve (Fig. 4D, Table S1). Importantly, the values developed using RI data in the absence of drugs allowed good fitting of experimental dose-response curves, including the upward inflection that is apparent in the experimental data and that is predicted by the model for these n_T and c values (Fig. 5A).

Since c=2 for protease predicts a slope approaching 2 at high [D], the model does not explain m>2 for some PIs or the sharp upward inflection at high [D]. Therefore, we tested the model using PIs with m~2. For the wild-type dose-response curves, we considered only the initial linear part as described previously (12) and excluded the two data points at high [D]. n_T=9–15, σ=4–6, c=2 all fit the wild-type curves. With n_T=12, σ=5, c=2, we obtained K_d=0.0068 μM, 0.039 μM, and 0.021 μM for lopinavir (LPV), nelfinavir (NFV), and amprenavir (APV), respectively (Fig. 5B). The introduction of σ for protease improved the fitting of the RI curve slightly (Fig. 4E, Table S1).

Having established values of n_T and c that allow fitting of both RI data and dose-response curves for wild-type virus, we next examined the effect of decreasing n_F on the dose-response curves. As predicted, the dose-response curves for NNRTIs shifted only slightly to the left with increasing f_m. The experimental data fit the model predictions with r^2>0.94 for each of the curves obtained for EFV and ETR (Fig. 5A, Supplementary Note 2). For NVP, the r^2 values were >0.90 (Fig. 5A). For PIs, the model predicts a substantial left shift of the dose-response curves with increasing f_m. Again, the experimental data fit the model predictions well with r^2>0.87 for all drug curves with various f_m (Fig. 5B, Supplementary Note 2). These results are consistent with the fractional occupancy of RT or protease required for inhibiting replication. The finding that the IC_{50} decreased with decreasing n_F for PIs can be understood by considering that virus particles with lower n_F are more easily inhibited, since fewer protease molecules must be bound by the drug in order to reduce the number of unbound protease molecules to below c. This result is also consistent with reports that the threshold activity of protease necessary for infectivity is small relative to the total protease activity per virion (25). In contrast, most of the RT molecules present are required for viral replication. Therefore, deceasing n_F had minimal effect on the IC_{50} of the NNRTIs.

Taken together, these results suggest that the participation of multiple copies of RT and protease in the processes of reverse transcription and virion maturation, respectively, results in a form of intermolecular cooperativity that is manifested as steeper dose-response curves for the NNRTIs and PIs. The cooperative curves can be fit using the critical subset model without the need to postulate interactions between the active sites of individual enzyme molecules.

Analysis of the dose-response curves for InSTIs and NRTIs against phenotypically-mixed viruses

The InSTIs and the NRTIs exhibit slopes close to 1 (12). Unlike NNRTIs and PIs, these drugs target reactions in which a *single* molecular complex of one enzyme with viral nucleic acid mediates a critical step. For the InSTIs, the inhibited process is performed by precisely one molecular complex per infected cell, consisting of an integrase tetramer bound to the ends of the viral genome (26, 27). There is no possibility for intermolecular cooperativity because only a single drug target per virus mediates the targeted reaction. Other integrase molecules present in the preintegration complex are not targeted by InSTIs and are irrelevant. Similar reasoning can be applied to RT by breaking reverse transcription into individual steps, each consisting of attachment of one nucleotide. The NRTIs target a single enzyme:nucleic acid complex per infected cell, namely the RT molecule that is adding the next nucleotide to the viral cDNA (17). Other RT molecules in the reverse transcription complex are irrelevant and are not targeted. When a single target mediates the critical reaction (n_T=c=1), Equation 3 reduces to the median effect equation (Equation 2) with m=1 (Fig. 2C–D), consistent with the experimental observations (12). The model predicts that phenotypic mixing should not affect m or IC_{50} because non-functional complexes are irrelevant for drug inhibition and functional complexes are inhibited by drug in the same manner for both wild-type and phenotypically mixed viruses.

To test these predictions, we generated phenotypically mixed virions in which a fraction of the integrase or RT molecules had the inactivating catalytic site mutations D64E or D185N, respectively (23, 24). Drug susceptibility was measured using the single round infectivity assay. The slopes were close to 1 and exhibited minimal change against modulated viruses as predicted by the model (Fig. 6, S4). The IC_{50} values for the InSTIs raltegravir (RAL) and elvitegravir (ELV) against phenotypically-mixed virions were unchanged (Fig. 6A). For all NRTIs except for zidovudine, there was no decrease in IC_{50}, consistent with the model. Interestingly, IC_{50} values for most NRTIs such as lamivudine (3TC) and abacavir (ABC) increased slightly relative to wild-type at f_m=0.5 (Fig. 6B, S4). The dose-response curves for zidovudine represented an exception, as the IC_{50} was dramatically decreased as f_m increased (Fig. S4). This increased sensitivity may reflect reduced excision of zidovudine when there are fewer active RT molecules (21). With this exception, no InSTI and NRTIs showed decreased IC_{50} when some copies of the relevant enzymes carried inactivating mutations (Fig. 6, S4). This behavior is in sharp contrast to the NNRTIs and PIs, drugs for which phenotypically mixed virions invariably showed decreased IC_{50}. Both sets of observations are consistent with the critical subset model.

Discussion

Steep dose-response curves generally reflect positive cooperativity. In the classical Hill model, a slope >1 reflects cooperative binding of multiple ligands to a multivalent receptor. However, RT and protease have only one binding site for NNRTIs and PIs, respectively, and extensive kinetics studies with purified RT and protease have not provided evidence for cooperativity. Rather, the high slopes of NNRTIs and PIs in infectivity assays reflect unique aspects of the inhibition of viral replication that are not apparent in the behavior of the isolated enzymes.

Here we present a critical subset model that provides a molecular explanation for these steep dose-response curves. We hypothesized that within a given infected cell or virus particle, the viral proteins targeted by a drug behave as a set of linked receptor sites whose fractional occupancy determines whether the relevant step in the virus life cycle is completed before irreversible decay processes intervene. When multiple copies of a target are involved in the inhibited reaction, there exists a form of intermolecular cooperativity that does not depend on alterations in the binding properties of individual sites. This model predicts slopes >1 for NNRTIs and PIs because multiple copies of RT and protease are involved in the processes inhibited by these drugs, and a critical subset of these molecules are required for viral replication. The model successfully predicted shifts in the dose-response curves against viruses with decreased n_F. For NRTIs and InSTIs, only one copy of RT or integrase is relevant to the inhibited reaction. In this situation, $m \sim 1$ is predicted, as is observed experimentally.

According to the model, slope is determined by n_T and c. There are ~5000 copies of Gag per virion, and the ratio of Gag-Pol to Gag is 1:10~1:20 (28, 29). Thus if the Gag-Pol polypeptides are converted with 100% efficiency into functional dimeric RT and protease enzymes, there would be a maximum of 125–250 copies of these enzymes per virion. The n_T values for RT and protease obtained here are smaller, perhaps reflecting inefficiencies in the assembly of functional enzymes and additional complexities in the relevant reactions. The n_T and c parameters in this model are *apparent* numbers that allow description of the relevant reactions in terms of a simple model that does not capture the full complexity of the processes of reverse transcription and virion maturation. In addition, n_T and c refer only to enzyme molecules located in the microenvironment where the reaction occurs. For these reasons, n_T and c may differ from the actual physical number of RT or protease molecules present.

Since n_T and c for a given drug target should be constant, the model does not explain slope differences within the PI class. The model particularly cannot explain dose-response curves for PIs with $m>2$, since $c=2$ for protease predicts a maximum slope of 2. We hypothesize that drug-to-drug variability in m for PIs may reflect the complexity of viral maturation, which involves multiple molecular states of the enzyme acting on multiple distinct substrates (30). The protease domains of adjacent Gag-Pol precursor proteins must first dimerize to form an active protease enzyme, which then carries out intramolecular cleavages to liberate itself from the Gag-Pol precursor protein. Ultimately free protease dimers complete the remaining cleavages of the Gag and Gag-Pol precursor proteins (31). The embedded protease is less sensitive to PIs than the mature, free enzyme (30, 31). The effective substrate concentration may also differ for intramolecular and intermolecular reactions. Different PIs may preferentially inhibit distinct molecular forms of protease for which n_T and c are different, resulting in slope differences. In addition, virions generated in the presence of PIs may be blocked at subsequent steps such as reverse transcription (32). Thus, unlike other antiretroviral drugs, PIs affect multiple steps in the life cycle, possibly with different n_T and c values. These complexities may explain the upward inflection of PI dose-response curves at high [D].

The concepts developed here can be applied to other drug classes and other viruses. However, additional factors may complicate the analysis. For drugs affecting HIV-1 entry, the targets are trimeric, and interactions within and between trimers must be considered. One particularly unique aspect of HIV-1 RT, protease, and integrase inhibitors is that they target enzymes that are present within the virion or that are assembled from precursor polyproteins present within the virion. In this situation, constraints inherent in virion assembly limit heterogeneity (σ) in n_T. As shown here, heterogeneity flattens dose-response curves. Thus in the case of viruses for which the drug targets are expressed and act within infected cells,

heterogeneity in the number of enzymes per cell may obscure the cooperativity that is expected when multiple copies of a drug target act together to complete a step in the life cycle.

A variety of elegant models describing steep dose-response curves for ion channels and other multivalent receptors have been developed (16, 33–35), but models to explain cooperative dose-response curves for antiviral drugs have not been described. It is possible that other models will be developed to explain the complex dose-effect relationships for antiretroviral drugs. For example, saturable drug binding to alternative intracellular sites could result in an upward inflection within a small concentration range above the concentration that saturates the alternative sites. However, a model such as the one described here would still be needed to explain slopes >1 in other regions of the dose-response curve. Although the overall slopes for NRTIs are close to 1, there are subtle inflections in the dose-response curves for some NRTIs (Fig. 6B, S4). These may in part reflect binding to alternative intracellular sites or the reactions needed to produce the active triphosphate forms of the NRTIs. Nevertheless, the fact that slope varies in a class-specific way despite large intraclass differences in structure suggests that the slope parameter is a direct reflection of the mechanism of inhibition, as in the model described here.

The critical subset model clearly represents an oversimplification of a very complex problem. Nevertheless, it explains the steep dose-response curves of NNRTIs and PIs without assuming that the binding of drug to one site affects the K_d of binding to other sites. A steep slope means that small increases in drug concentration above the IC_{50} can produce large increases in antiviral activity, permitting extremely high levels of inhibition in the clinical concentration range. Thus the present study provides a conceptual framework for understanding the high antiviral activity of NNRTIs and PIs, drugs that form the basis of successful HIV-1 treatment, and provides important insights to the characteristics of good targets for antiviral drugs.

Materials and Methods

Detailed descriptions of experimental Materials and Methods are available in the Supplementary Material.

Analysis of relative infectivity (*RI*) curves

The *RI* values of recombinant viruses generated with different f_m were obtained by normalizing to the infectivity of the wild-type virus. Theoretical *RI* values were calculated for given values of n_T and c using the binomial distribution (Equation 6). This analysis required a consideration of the subunit stoichiometry of the relevant multimeric targets. The probability of obtaining a functional multimer (P_f) is a function of f_m, the valence of the multimer, and the functional status of mixed multimers. For example, the enzymatic activity of protease requires the D25 residues from both subunits of the dimer (18). Thus for protease, $P_f = (1-f_m)^2$. For RT, although a D185N mutation in the p66 subunit abolishes activity, a D185N mutation in the p51 subunit has no effect on enzyme activity (23). Thus for RT, $P_f = (1-f_m)^2 + f_m(1-f_m) = 1-f_m$. To estimate the apparent n_T and c values required for virus replication, experimental *RI* curves were fitted with theoretical curves predicted by the model (Equation 6) using various n_T and c, and r^2 values were obtained for both *RI* and log *RI* (Fig. 4B–C). While fitting using the linear scale puts more weight on higher *RI* values, fitting using the log scale emphasizes lower *RI* values. Pairs of n_T and c values giving the best five average r^2 values with both methods were used for further analysis of dose-response curves (Fig. 4A). To estimate the 95% confidence interval for n_T and c, we bootstrapped the experimental *RI* curves 1000 times by perturbing the mean by a random value centered around the mean with standard deviation equal to the SEM of the data.

Analysis of dose-response curves

Dose-response curves for virus stocks with various f_m were obtained by normalizing to the %GFP$^+$ cells without drug treatment. When necessary, the IC_{50} and slope based on the median effect equation (Equation 1) were calculated through least-squares regression analysis as described previously (12). To refine the values for n_T and c and find the approximate K_d, we used the pairs of n_T and c values estimated from RI curves as a start point in a systematic search for values of σ and K_d that would fit best with the experimental dose-response curves for NNRTIs or PIs against wild-type viruses (Equation 4). Values of $\sigma > n_T/2$ were not allowed. Once an optimal set of n_T, c, σ, and K_d values was obtained, these values were used to predict theoretical dose-response curves for phenotypically mixed virions (Fig. 4A). The r^2 values representing fitting of predicted theoretical dose-response curves to the experimental curves were then calculated. Note that it is not necessary to consider the binding of a drug to the inactive enzyme for calculation of f_a (Supplementary Note 3).

Mathematical modeling and statistical analyses

All theoretical curve simulations, calculations, curve fitting and statistical analyses were performed using Matlab version 7.1 (The MathWorks) or Microsoft Office Excel 2003.

Supplementary Material

Refer to Web version on PubMed Central for supplementary material.

Acknowledgments

We thank the AIDS Research and Reference Reagent Program of the US National Institutes of Health and Merck for providing anti-HIV-1 drugs. We thank Drs. J. Liu, E. Freire, and X. Yu for helpful discussions. We thank Drs. J. Siliciano, J. Blankson, and C. Durand for helpful review of the manuscript.

Funding: This work was supported by the US National Institutes of Health grant AI081600 and by the Howard Hughes Medical Institute.

References and Notes

1. Gulick RM, Mellors JW, Havlir D, Eron JJ, Gonzalez C, McMahon D, Richman DD, Valentine FT, Jonas L, Meibohm A, Emini EA, Chodakewitz JA. Treatment with Indinavir, Zidovudine, and Lamivudine in Adults with Human Immunodeficiency Virus Infection and Prior Antiretroviral Therapy. N Engl J Med. 1997; 337:734–739. [PubMed: 9287228]
2. Hammer SM, Squires KE, Hughes MD, Grimes JM, Demeter LM, Currier JS, Eron JJ Jr, Feinberg JE, Balfour HH Jr, Deyton LR, Chodakewitz JA, Fischl MA. A Controlled Trial of Two Nucleoside Analogues Plus Indinavir in Persons with Human Immunodeficiency Virus Infection and CD4 Cell Counts of 200 Per Cubic Millimeter Or Less. AIDS Clinical Trials Group 320 Study Team. N Engl J Med. 1997; 337:725–733. [PubMed: 9287227]
3. Perelson AS, Essunger P, Cao Y, Vesanen M, Hurley A, Saksela K, Markowitz M, Ho DD. Decay Characteristics of HIV-1-Infected Compartments during Combination Therapy. Nature. 1997; 387:188–191. [PubMed: 9144290]
4. Staszewski S, Morales-Ramirez J, Tashima KT, Rachlis A, Skiest D, Stanford J, Stryker R, Johnson P, Labriola DF, Farina D, Manion DJ, Ruiz NM. Efavirenz Plus Zidovudine and Lamivudine, Efavirenz Plus Indinavir, and Indinavir Plus Zidovudine and Lamivudine in the Treatment of HIV-1 Infection in Adults. Study 006 Team. N Engl J Med. 1999; 341:1865–1873. [PubMed: 10601505]
5. Panel on Antiretroviral Guidelines for Adult and Adolescents, Guidelines for the use of Antiretroviral Agents in HIV-1-Infected Adults and Adolescents. DHHS. Jan.2011 :1–166.
6. Larder BA, Darby G, Richman DD. HIV with Reduced Sensitivity to Zidovudine (AZT) Isolated during Prolonged Therapy. Science. 1989; 243:1731–1734. [PubMed: 2467383]

7. Coffin JM. HIV Population Dynamics in Vivo: Implications for Genetic Variation, Pathogenesis, and Therapy. Science. 1995; 267:483–489. [PubMed: 7824947]
8. Wei X, Ghosh SK, Taylor ME, Johnson VA, Emini EA, Deutsch P, Lifson JD, Bonhoeffer S, Nowak MA, Hahn BH, Saag MS, Shaw GM. Viral Dynamics in Human Immunodeficiency Virus Type 1 Infection. Nature. 1995; 373:117–122. [PubMed: 7529365]
9. Ho DD, Neumann AU, Perelson AS, Chen W, Leonard JM, Markowitz M. Rapid Turnover of Plasma Virions and CD4 Lymphocytes in HIV-1 Infection. Nature. 1995; 373:123–126. [PubMed: 7816094]
10. Wodarz D, Nowak MA. Mathematical Models of HIV Pathogenesis and Treatment. Bioessays. 2002; 24:1178–1187. [PubMed: 12447982]
11. Ribeiro RM, Bonhoeffer S, Nowak MA. The Frequency of Resistant Mutant Virus before Antiviral Therapy. AIDS. 1998; 12:461–465. [PubMed: 9543443]
12. Shen L, Peterson S, Sedaghat AR, McMahon MA, Callender M, Zhang H, Zhou Y, Pitt E, Anderson KS, Acosta EP, Siliciano RF. Dose-Response Curve Slope Sets Class-Specific Limits on Inhibitory Potential of Anti-HIV Drugs. Nat Med. 2008; 14:762–766. [PubMed: 18552857]
13. Hill AV. The Possible Effects of the Aggregation of the Molecules of Haemoglobin on its Dissociation Curves. J Physiol. 1910; 40:iv–vii.
14. Holpord NHG, Scheiner LB. Understanding the Dose-effect Relationship: Clinical Applications of Pharmacokinetic-pharmacodynamic Models. Clin Pharmacokinet. 1981; 6:429–453. [PubMed: 7032803]
15. Chou TC. Theoretical Basis, Experimental Design, and Computerized Simulation of Synergism and Antagonism in Drug Combination Studies. Pharmacol Rev. 2006; 58:621–681. [PubMed: 16968952]
16. Weiss JN. The Hill Equation Revisited: Uses and Misuses. FASEB J. 1997; 11:835–841. [PubMed: 9285481]
17. Kohlstaedt LA, Wang J, Friedman JM, Rice PA, Steitz TA. Crystal Structure at 3.5 A Resolution of HIV-1 Reverse Transcriptase Complexed with an Inhibitor. Science. 1992; 256:1783–1790. [PubMed: 1377403]
18. Miller M, Schneider J, Sathyanarayana BK, Toth MV, Marshall GR, Clawson L, Selk L, Kent SB, Wlodawer A. Structure of Complex of Synthetic HIV-1 Protease with a Substrate-Based Inhibitor at 2.3 A Resolution. Science. 1989; 246:1149–1152. [PubMed: 2686029]
19. Mitsuya H, Maeda K, Das D, Ghosh AK. Development of Protease Inhibitors and the Fight with Drug-Resistant HIV-1 Variants. Adv Pharmacol. 2008; 56:169–197. [PubMed: 18086412]
20. Hoffman A, Goldberg A. The Relationship between Receptor-Effector Unit Heterogeneity and the Shape of the Concentration-Effect Profile: Pharmacodynamic Implications. J Pharmacokinet Biopharm. 1994; 22:449–468. [PubMed: 7473076]
21. Ambrose Z, Julias JG, Boyer PL, Kewalramani VN, Hughes SH. The Level of Reverse Transcriptase (RT) in Human Immunodeficiency Virus Type 1 Particles Affects Susceptibility to Nonnucleoside RT Inhibitors but Not to Lamivudine. J Virol. 2006; 80:2578–2581. [PubMed: 16474164]
22. Yang X, Kurteva S, Ren X, Lee S, Sodroski J. Stoichiometry of Envelope Glycoprotein Trimers in the Entry of Human Immunodeficiency Virus Type 1. J Virol. 2005; 79:12132–12147. [PubMed: 16160141]
23. Le Grice SF, Naas T, Wohlgensinger B, Schatz O. Subunit-Selective Mutagenesis Indicates Minimal Polymerase Activity in Heterodimer-Associated p51 HIV-1 Reverse Transcriptase. EMBO J. 1991; 10:3905–3911. [PubMed: 1718745]
24. Hazuda DJ, Felock P, Witmer M, Wolfe A, Stillmock K, Grobler JA, Espeseth A, Gabryelski L, Schleif W, Blau C, Miller MD. Inhibitors of Strand Transfer that Prevent Integration and Inhibit HIV-1 Replication in Cells. Science. 2000; 287:646–650. [PubMed: 10649997]
25. Rose JR, Babe LM, Craik CS. Defining the Level of Human Immunodeficiency Virus Type 1 (HIV-1) Protease Activity Required for HIV-1 Particle Maturation and Infectivity. J Virol. 1995; 69:2751–2758. [PubMed: 7535864]
26. Pandey KK, Bera S, Zahm J, Vora A, Stillmock K, Hazuda D, Grandgenett DP. Inhibition of Human Immunodeficiency Virus Type 1 Concerted Integration by Strand Transfer Inhibitors

which Recognize a Transient Structural Intermediate. J Virol. 2007; 81:12189–12199. [PubMed: 17804497]

27. Hare S, Gupta SS, Valkov E, Engelman A, Cherepanov P. Retroviral Intasome Assembly and Inhibition of DNA Strand Transfer. Nature. 2010; 464:232–236. [PubMed: 20118915]
28. Briggs JA, Simon MN, Gross I, Krausslich HG, Fuller SD, Vogt VM, Johnson MC. The Stoichiometry of Gag Protein in HIV-1. Nat Struct Mol Biol. 2004; 11:672–675. [PubMed: 15208690]
29. Jacks T, Power MD, Masiarz FR, Luciw PA, Barr PJ, Varmus HE. Characterization of Ribosomal Frameshifting in HIV-1 Gag-Pol Expression. Nature. 1988; 331:280–283. [PubMed: 2447506]
30. Pettit SC, Clemente JC, Jeung JA, Dunn BM, Kaplan AH. Ordered Processing of the Human Immunodeficiency Virus Type 1 GagPol Precursor is Influenced by the Context of the Embedded Viral Protease. J Virol. 2005; 79:10601–10607. [PubMed: 16051852]
31. Pettit SC, Everitt LE, Choudhury S, Dunn BM, Kaplan AH. Initial Cleavage of the Human Immunodeficiency Virus Type 1 GagPol Precursor by its Activated Protease Occurs by an Intramolecular Mechanism. J Virol. 2004; 78:8477–8485. [PubMed: 15280456]
32. Muller B, Anders M, Akiyama H, Welsch S, Glass B, Nikovics K, Clavel F, Tervo HM, Keppler OT, Krausslich HG. HIV-1 Gag Processing Intermediates Trans-Dominantly Interfere with HIV-1 Infectivity. J Biol Chem. 2009; 284:29692–29703. [PubMed: 19666477]
33. Agneter E, Singer EA, Sauermann W, Feuerstein TJ. The Slope Parameter of Concentration-Response Curves used as a Touchstone for the Existence of Spare Receptors. Naunyn Schmiedebergs Arch Pharmacol. 1997; 356:283–292. [PubMed: 9303563]
34. Castrignano T, Aluffi-Pentini F, Parisi V. A Novel Parameter to Estimate the Minimum Number of Bound Ligands Needed to Activate an Ion Channel. J Theor Biol. 1999; 199:97–103. [PubMed: 10419762]
35. Michel D. Cooperative Equilibrium Curves Generated by Ordered Ligand Binding to Multi-Site Molecules. Biophys Chem. 2007; 129:284–288. [PubMed: 17643734]

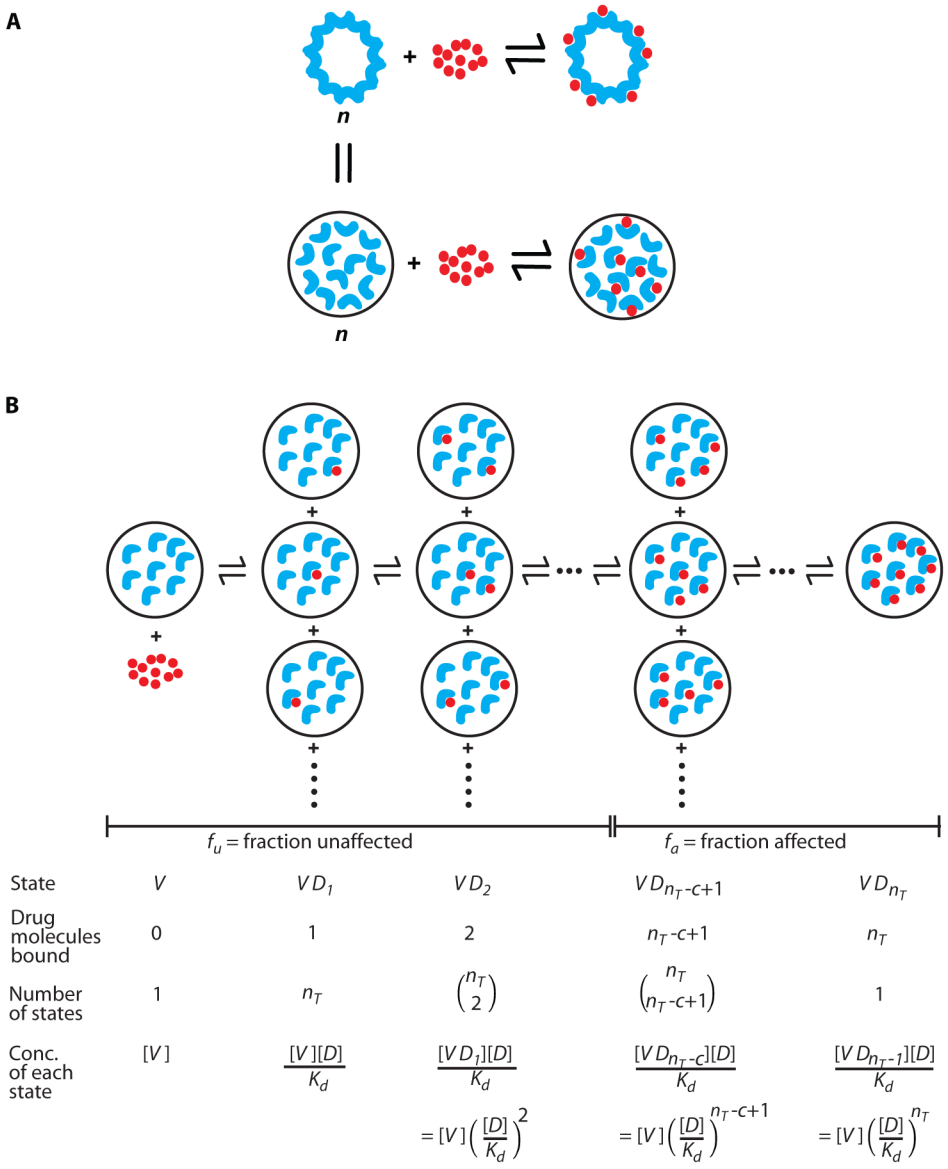

State	V	VD_1	VD_2	VD_{n_T-c+1}	VD_{n_T}
Drug molecules bound	0	1	2	n_T-c+1	n_T
Number of states	1	n_T	$\binom{n_T}{2}$	$\binom{n_T}{n_T-c+1}$	1
Conc. of each state	$[V]$	$\frac{[V][D]}{K_d}$	$\frac{[VD_1][D]}{K_d}$ $= [V]\left(\frac{[D]}{K_d}\right)^2$	$\frac{[VD_{n_T-c}][D]}{K_d}$ $= [V]\left(\frac{[D]}{K_d}\right)^{n_T-c+1}$	$\frac{[VD_{n_T-1}][D]}{K_d}$ $= [V]\left(\frac{[D]}{K_d}\right)^{n_T}$

Figure 1.

The critical subset model. **(A)** A virion (or virally infected cell) can be viewed as a multivalent receptor containing n identical copies of a given drug target such as HIV-1 protease. Although not physically linked to one another, these copies are spatially constrained within the virus particle or infected cell. **(B)** Sequential binding of a protease inhibitor (red circle) to the protease dimers (blue crescents) within a virion. The concentrations of the various bound states can be determined by the law of mass action, assuming a single unchanging dissociation constant, K_d. Assuming that successful completion of the relevant step in the virus life cycle requires a critical number c of functional unbound copies of the drug target, f_a can be computed as the concentration of inhibited states divided by the concentration of all possible states (Equation 3). f_u is equal to $1-f_a$. Similar arguments can be applied to RT except that the RT molecules are present within the reverse transcription complex in an infected cell.

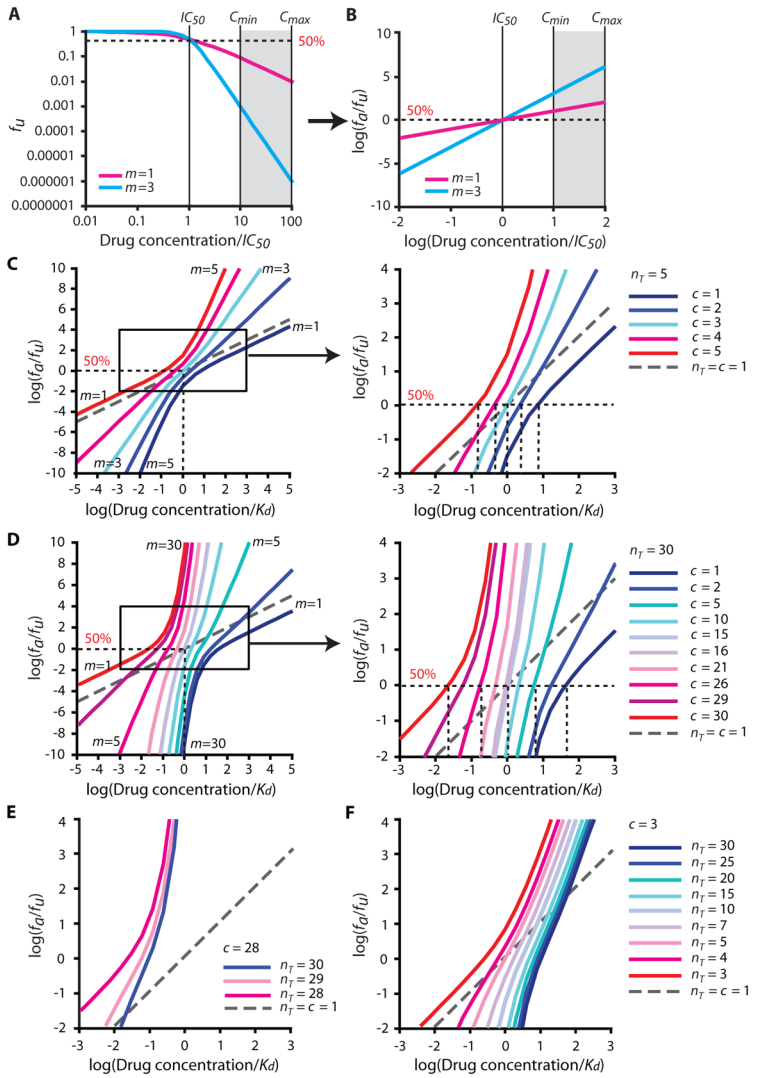

Figure 2.

Steep dose-response curves predicted by the critical subset model. **(A)** Hypothetical log-log plot of f_u vs. drug concentration based on the median-effect model for drugs with different m values. The strong impact of slope on the suppression of infectivity is apparent at high drug concentrations. Drug concentrations are normalized by IC_{50}. The dotted line represents 50% inhibition. **(B)** Hypothetical median effect plot [log (f_a/f_u) vs. log drug concentration] (Equation 1) of the curves shown in Figure 2A. The m value is the slope of the line. **(C, D)** Hypothetical median effect plots of dose-response curves generated using the critical subset model assuming n_T = 5 **(C)** or 30 **(D)** and values of c ranging from 1 to n_T. Concentrations are normalized by K_d. The right panel is an expansion of the indicated area in the left panel. As c increases, IC_{50} decreases, and slope increases at concentrations above the IC_{50}, but decreases at concentrations below the IC_{50}. A standard non-cooperative dose-response curve with m=1 (n_T=c=1) is also shown (gray dashed line). **(E, F)** Hypothetical median effect plots of dose-response curves generated using the critical subset model with values of n_T ranging from c to 30, and c=28 **(E)** or 3 **(F)**. As n_T decreases, the dose-response curves shift to the left.

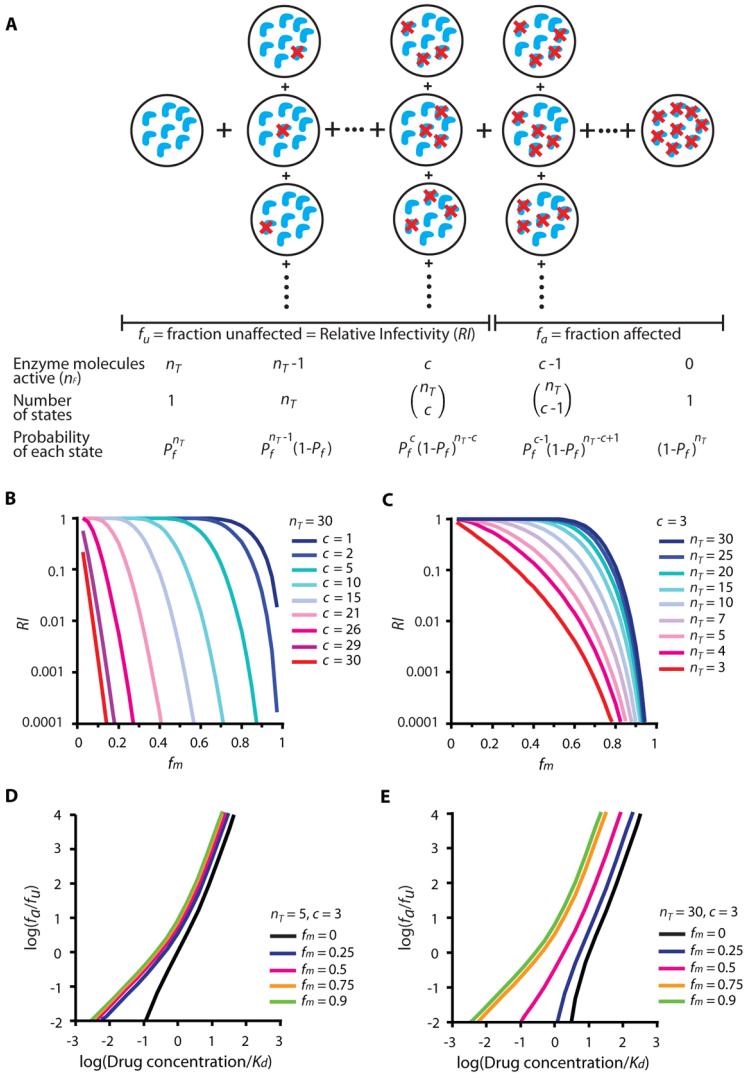

Figure 3.

Effect of reductions in n_F on the dose-response curves for antiviral drugs. **(A)** Relative infectivity (*RI*) of phenotypically-mixed virions. Consider a population of virions with the same n_T but various numbers of active (n_F, blue crescents) and inactive protease molecules (crescents with red cross). P_f is the probability of obtaining a function protease molecule for a given f_m. The probability of getting n_F copies of functional enzyme molecules ($P(n_F)$) as a function of n_T, c, and P_f can be calculated using Equation 6. The *RI* of a population of phenotypically-mixed virions is the sum of the probabilities of all the viruses with $n_F \geq c$. **(B, C)** Hypothetical *RI* plots [*RI* vs. f_m] for protease with $n_T = 30$ and various values of c **(B)**, or $c=3$ and various values of n_T **(C). (D, E)** Hypothetical median effect plots of dose-response curves for PIs against viruses with $c=3$, $n_T = 5$ **(D)** or c=3, $n_T = 30$ **(E)**, and various f_m values. Concentrations are normalized by K_d. The change in IC_{50} is larger when c is proportionally small relative to n_T **(E)**.

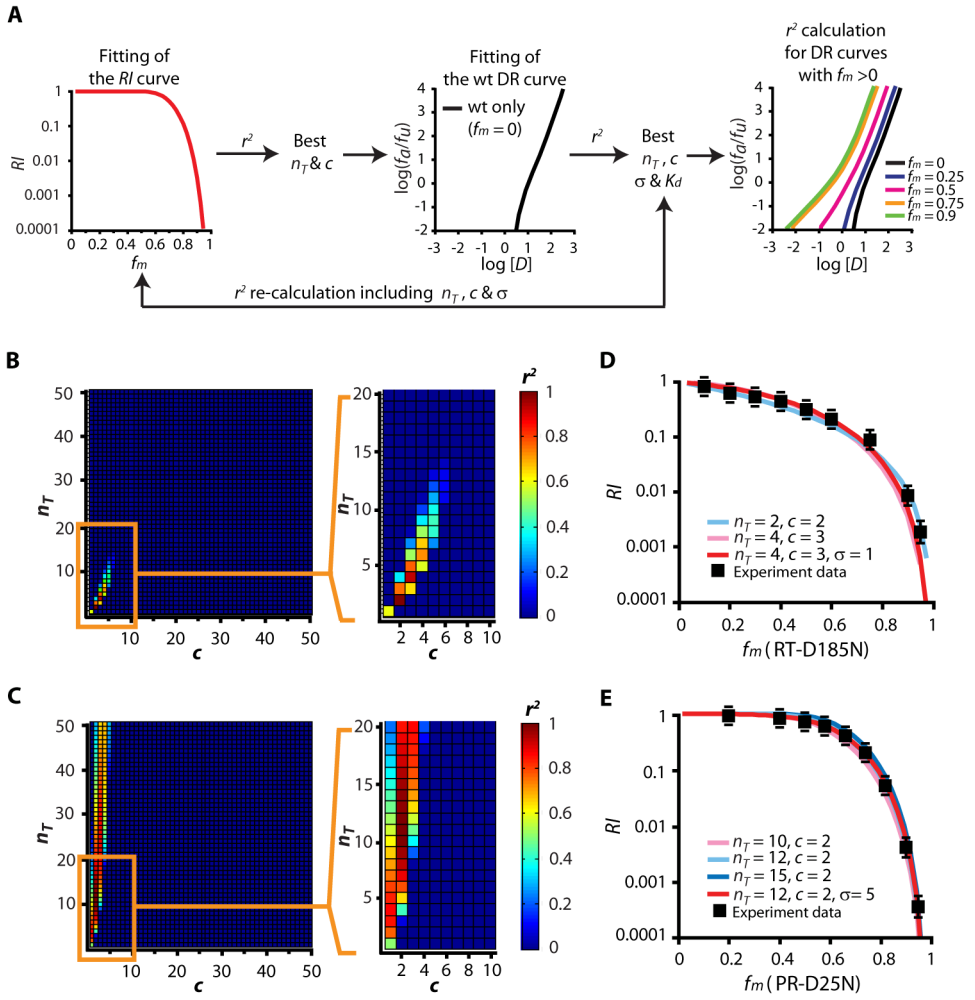

Figure 4.

Experimental validation of the critical subset model. **(A)** Algorithm for model validation from experimental data. Curves describing the dependence of the relative infectivity (*RI*) of phenotypically-mixed virions on f_m in the absence of drug were first obtained. Experimental *RI* curves were fitted with theoretical curves (Equation 6) using various n_T and c values, and r^2 values were calculated. The n_T and c values that gave the best five r^2 values were used in the next step. These pairs of n_T and c values were used as a start point in a systematic search for values of σ and K_d that allowed the best fit with dose-response curves for NNRTIs or PIs against wild-type viruses. The r^2 values for the fitting of the *RI* curves were recalculated with the resulting sets of n_T, c, and σ values. Once an optimal set of n_T, c, σ, and K_d values was obtained, these values were used to predict dose-response curves for phenotypically mixed virions. The r^2 values representing the fitting of predicted dose-response curves to the experimental curves were then calculated. **(B, C)** Estimates of n_T and c for RT **(B)** and protease **(C)**. The r^2 values for fitting of RT and protease *RI* curves to each pair of n_T and c values are shown. Red squares indicate r^2 close to 1, and blue squares indicate r^2 <0.2. **(D, E)** *RI* curves for RT **(D)** and protease **(E)**. Theoretical *RI* curves predicted by the critical subset model are plotted as a function of f_m (solid lines). The actual experimental data are shown in black squares. The *RI* of a given viral stock was calculated by normalization to the infectivity of the viral stock carrying only wild-type enzyme. Each data point represents the mean ± SEM from >3 experiments.

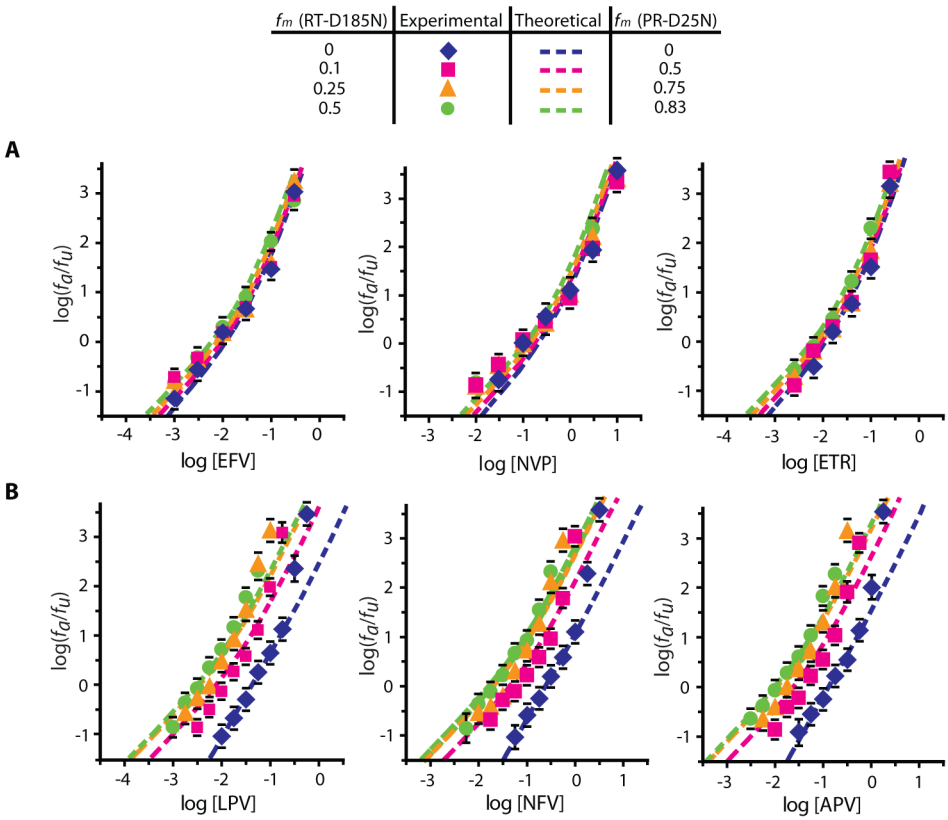

Figure 5.

Effect of phenotypic mixing on dose-response curves for NNRTIs and PIs. **(A)** Median effect plots of theoretical (dashed lines) and experimental (solid markers) dose-response curves for the NNRTIs EFV, NVP, and ETR with wild-type and phenotypically mixed virions. The dose-response curves for phenotypically mixed virion preparations exhibited the expected slight decrease in IC_{50} compared to wild-type virions. **(B)** Median effect plots of theoretical (dashed lines) and experimental (solid markers) dose-response curves for the PIs LPV, NFV, and APV with wild-type and phenotypically mixed virions. The two data points at high drug concentrations for the wild-type dose-response curves were excluded from the fitting. Dose-response curves for phenotypically mixed virion preparations showed the expected left shift with increasing f_m. Each data point represents the mean ± SEM from >3 experiments.

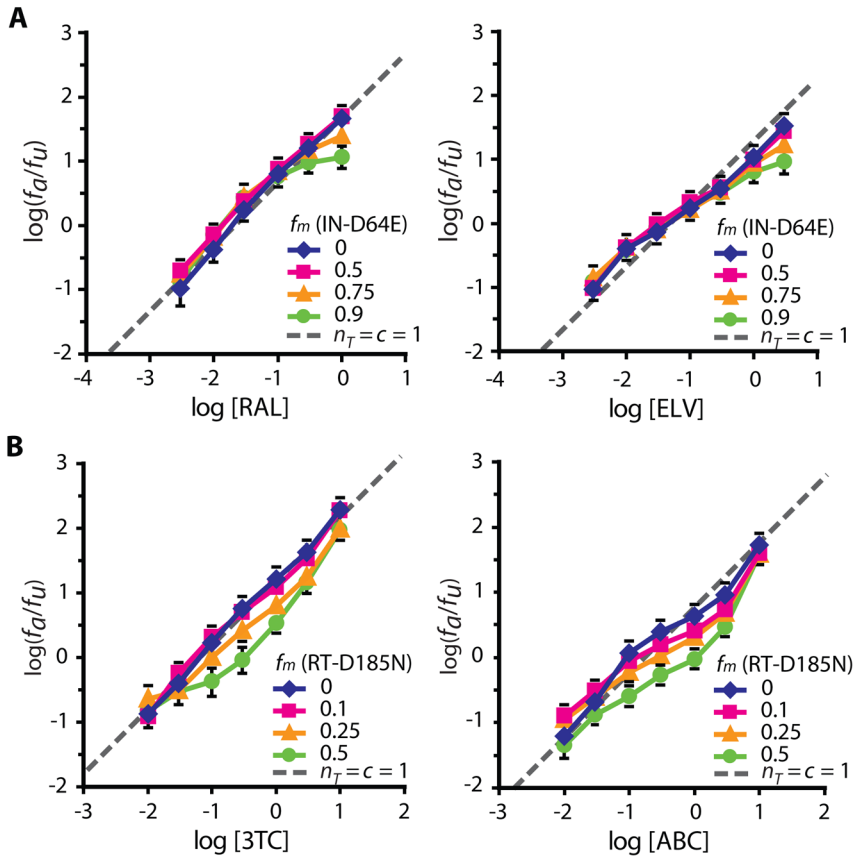

Figure 6.

Effect of phenotypic mixing on dose-response curves for InSTIs and NRTIs. **(A)** Dose-response curves for the InSTIs RAL and ELV against wild-type virus and viruses generated with increasing fractions of the D64E mutant plasmid. The IC_{50} and slope did not change with increasing f_m. As previously described (13), the flattening of the dose-response curves at high concentrations of InSTIs and high f_m may reflect low level GFP expression from unintegrated proviruses. **(B)** The dose-response curves for the NRTIs 3TC and ABC against wild-type virus and viruses generated with increasing fractions of the D185N mutant plasmid. There was a 2–4 fold increase in IC_{50} and minimal change in slope with increasing f_m. Each data point represents the mean ± SEM from >3 experiments.

Table 1

Glossary of abbreviations.

f_a	Fraction of viruses or infection events affected by the drug
f_u	Fraction of viruses or infection events unaffected by the drug
$[D]$	Drug concentration
IC_{50}	Drug concentration that leads to 50% inhibition
m	Slope parameter or Hill coefficient
K_d	Dissociation constant for a drug binding to an individual target enzyme molecule
n_T	Average of total number of enzyme molecules per virion relevant to the inhibited reaction
c	Critical threshold number of functional enzyme molecules required for viral replication
$[V]$	Unbound virus concentration
σ	Standard deviation for n_T
n_{max}	Maximum total number of enzyme molecules per virion, usually set as $> n_T + 3\sigma$
n_i	Given total number of enzyme molecules per virion relevant to the inhibited reaction
f_m	Fraction of mutant plasmid transfected
P_f	Probability of obtaining functional enzyme multimers for a given f_m
n_F	Total number of functional target molecules per virion relevant to the inhibited reaction
RI	Relative infectivity of phenotypically-mixed viruses compared to the wild type virus